*Sensors and Materials*, Vol. 34, No. # (2022) 735–744
MYU Tokyo



S & M 2848

# Optical Characterization of Phosphate Glass with Additional Aluminum/Tin Impurities

Shun Akiyama,[1] Aika Sasaki,[1] Runa Nakajima,[1] Daichi Hasegawa,[1]
Kazuya Iizuka,[1] Shigetaka Kimura,[1] Yuki Akagami,[1]
Yuichi Kitagawa,[2] Osamu Hanaizumi,[1] and Wataru Kada[1*]

[1]Faculty of Science and Technology, Gunma University, 1-5-1 Tenjincho, Kiryu, Gunma 376-8515, Japan
[2]Horiba Techno Service Co., Ltd., 2 Miyanohigashi, Kisshoin, Minami-ku, Kyoto 601-8305, Japan

(Received October 17, 2021; accepted December 13, 2021)

***Keywords:*** phosphate glass, tin, aluminum, time-correlated single-photon counting, time-resolved emission spectra

The optical properties of phosphate glass (PG) with two different impurities, namely, aluminum and tin, were investigated. Broad white luminescence was observed from PGs with tin and aluminum impurities under deep ultraviolet exposure. Through emission and excitation spectroscopy and decay curve measurement, it is assumed that the origin of the broadband luminescence differs depending on the impurities introduced. In addition, time-resolved emission spectral analysis revealed the difference in decay constant at each wavelength. The results obtained in this study might give important information about two potential impurities of PG for a better understanding of background noise and the functions of widely used radio-photoluminescence (RPL) dosimeters.

## 1. Introduction

Phosphate glass with a silver activator is well recognized as an accurate personal dosimeter and is utilized at various nuclear facilities worldwide.[1–4] Phosphate glass with a silver activator responds to radiation exposure by generating electron–hole pairs in the glass substrate.[5,6] Electrons and holes diffuse in the glass, and $Ag^+$ ions in the phosphate capture electrons and $Ag^+$ is reduced to $Ag^0$. Holes form $Ag^{2+}$ after trapping by $PO_4$ tetrahedra in a slow migration process.[7,8] Ultraviolet photons are often utilized to excite two energy states of $Ag^{2+}$ and $Ag^0$, and excitation is relaxed by emitting radio-photoluminescence (RPL) photons, the intensity of which corresponds to the amount of radiation exposure.[9–11] RPL is stable and will not quickly disappear unless the dosimeter is annealed. A silver activator is excellent in covering a wide range of radiation, including high-energy photons and ionized particles with high efficiency. Unfortunately, the energy response of RPL phosphate glass (PG) is not tissue-equivalent. To obtain a better energy response curve, PG is combined with a thin film made of different elements, including copper, tin, and aluminum.

*Corresponding author: e-mail: kada.wataru@gunma-u.ac.jp
https://doi.org/10.18494/SAM3697

ISSN 0914-4935 
https://myukk.org/

Like silver, other elements can also be captured in the phosphate crystal structure. Previously, we reported copper activators in PG,[12] and those impurities might work as activators for different fluorescence functions.[13,14] Although different energy levels are often expected to be demonstrated for other activators, they might cause a fluorescence competition if the phosphates capture the impurities that act as activators in the glass substrate.

In this study, we investigated the optical properties of PG with two metal impurities, namely, tin (Sn) and aluminum (Al), that are utilized in the filter built into the RPL dosimeter. Unexpectedly, broadband luminescence was observed in both cases, which was not confirmed so far in the PG substrate. We evaluated the fluorescence and decay characteristics of the PG that exhibited an unknown fluorescence with Sn and Al impurities, which should be investigated further.

## 2. Materials and Methods

### 2.1 Fabrication of PG with tin and aluminum

Phosphate glasses with different impurities were manufactured by the procedure illustrated in Fig. 1.[12,15,16] On the basis of the composition ratio of the host material of the widely available RPL phosphate dosimeter, which is Na: 11.0, P: 31.5, O: 51.2, Al: 6.1, sodium metaphosphate powder [$NaPO_3$; Taihei Chemical Industrial Co., Ltd., >65%[17]] and aluminum metaphosphate powder [$Al(PO_3)_3$; Taihei Chemical Industrial Co., Ltd. >96.1%[17]] were mixed at a weight ratio of 1:1 ($NaPO_3$:$Al(PO_3)_3$ = 1:2.59 in molar ratio). The required amount of elemental powder, according to the purpose, was added thereto, and the mixture was sufficiently stirred. For example, 0.2 mol% AgCl was previously added to reproduce an RPL dosimeter (Ag: PG). By the same procedure, tin (Sn) impurities were introduced in powder form (New Met Ltd., 99.999%) with different molar ratios to form PG with tin impurities (Sn: PG). Also, aluminum was introduced in a similar powder form (Niraco Co., Ltd. 99.8%) to form PG with aluminum impurities (Al: PG). The agitated mixed powder was transferred to a porcelain crucible (Nikkato Corporation, B-2, 50 ml, $Al_2O_3$:44%, $SiO_2$:46%, maximum temperature: 1100°C), heated, and then melted at a maximum temperature of 1000 °C using a tabletop muffle furnace (Denken Hydental Co., Ltd., KDF-S70) in air atmosphere. The uniform heating conditions are 60 min for temperature rise and 60 min for temperature retention. After heating, the crucible was removed from the furnace, and the PG in the crucible was poured on an aluminum plate that was pre-

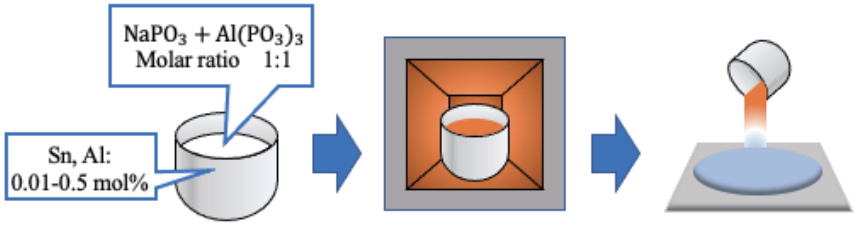


Fig. 1. (Color online) Fabrication of PG with different impurities.

heated to 400 °C in parallel with the crucible and naturally cooled in air atmosphere. The produced PG was cut into a shape according to its purpose using a band saw (K-100 manufactured by Hozan Co., Ltd.).

### 2.2 Optical measurement

Fluorescence from the prepared PG samples was first conveniently observed under a portable UV lamp with excitation center wavelengths of 254 and 365 nm. Light emission was almost negligible from both Al: PG and Sn: PG under 365 nm wavelength regardless of the concentrations of aluminum and tin. On the other hand, the samples showed bluish-white fluorescence under deep-UV irradiation with a center wavelength of 254 nm. The fluorescence intensity seems to increase with the aluminum or tin concentration. For Al: PG, the light intensity increased until the concentration reached 0.1 mol%, but no significant change in fluorescence intensity was observed thereafter. For Sn: PG, fluorescence could not be confirmed up to 0.02 mol%, but in samples with an additional concentration of 0.05 mol% or more, the fluorescence intensity tended to increase with the Sn concentration.

Then, two PG samples were evaluated using a UV-Vis modular spectrofluorometer (Fluorolog3, HORIBA Ltd.) and a lifetime fluorometer (DeltaFlex, HORIBA Ltd.). The spectrofluorometer has a Xe lamp as a light source and a photomultiplier as a detector. Spectra can be obtained in the range from 250 to 850 nm. The lifetime fluorometer is additionally utilized as a time-correlated single-photon counting (TCSPC) system for nanosecond-scale optical attenuation[18] and a multichannel scaling (MCS) system for microsecond-scale optical attenuation decay measurement.[19] Because of the limitation in the system configuration, two different wavelengths were employed for the measurements. A laser diode with a center wavelength of 507 nm was utilized for the TCSPC system, whereas another DC-LED with a center wavelength of 286 nm was employed for the MCS system.

## 3. Results

### 3.1 Excitation and emission spectroscopy

Figure 2 shows the results of photoexcitation and emission spectral mapping that were performed for PG with additional aluminum impurities of 0.1 mol% (Al: PG) and tin impurities of 0.5 mol% (Sn: PG). The samples of Sn: PG and Al: PG were selected at the impurity concentration where the brightest photoluminescence was observed in the optical investigation, as shown in Fig. 3. Figure 4 shows photoluminescence spectra of Al: PG and Sn: PG. Photoemission spectra were obtained with several excitation wavelengths for both Al: PG and Sn: PG. The graph's vertical axis represents the corrected fluorescence intensity, and the horizontal axis represents the emission wavelength. Broadband white luminescence was observed under the excitation light of 250–290 nm, and Al: PG and Sn: PG showed several peaks at around 370, 420, and 470 nm. The fluorescence spectral shapes of Al: PG and Sn: PG were different from each other.

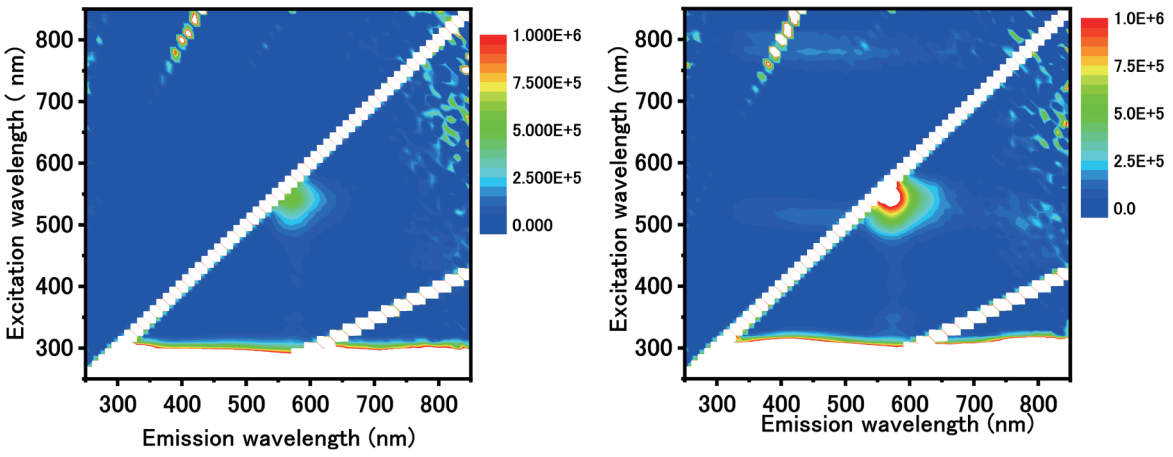


(a) (b)

Fig. 2. (Color online) Photoexcitation and emission spectral mapping from PG with (a) aluminum and (b) tin impurities.

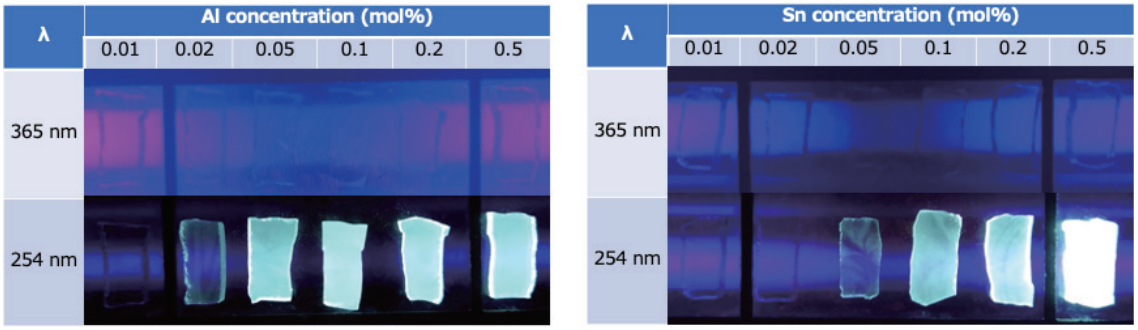


(a) (b)

Fig. 3. (Color online) Comparison of optical observations under 365 and 254 nm ultraviolet light of PG samples with additional (a) aluminum and (b) tin impurities with different molar ratios from 0.01 to 0.5 mol%.

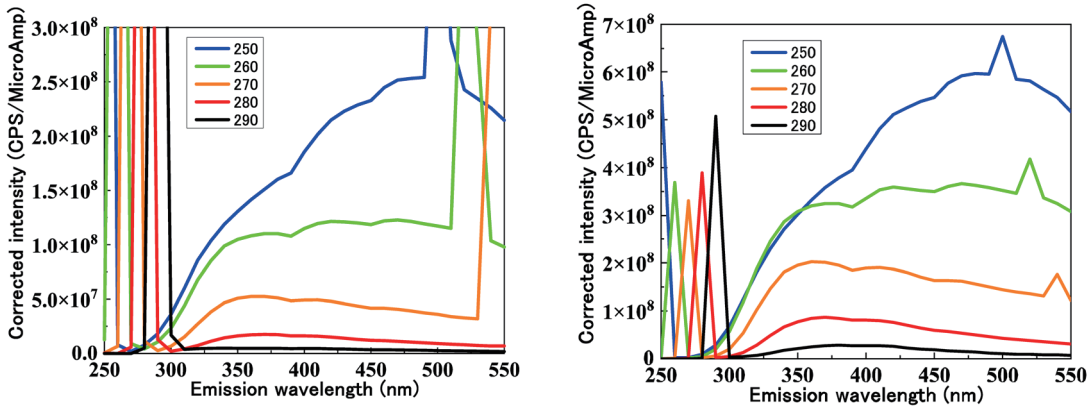


(a) (b)

Fig. 4. (Color online) Photoluminescence spectra from PG with (a) aluminum and (b) tin impurities.

The comparison of the overall fluorescence intensities of the two showed that Sn:PG has a higher value than Al:PG. In addition, under the excitation light of 500–540 nm, both Al: PG and Sn: PG showed emission peaks near 570 nm.

### 3.2 Decay curve analysis of PG with tin and aluminum impurities

Fluorescence attenuation curves were obtained for Al: PG and Sn: PG by utilizing an optical lifetime fluorometer system. Since multiple fluorescence peaks were observed, several wavelengths were measured. DC light from an LED with a center wavelength of 286 nm was utilized, and the DC light was turned off at a particular time period. Then, attenuation in the microsecond scale was observed (MCS mode). Figure 5 shows a comparison of two-lifetime fluorometer outputs. The results of fitting the obtained decay spectra through the MCS mode illustrate the difference between the two samples. Attenuation curves using the exponential functions of the three components are shown in Tables 1 and 2. Clearly, there is a significant difference in fluorescence lifetime on the order of microseconds between Al: PG and Sn: PG for emission wavelengths of 360, 420, and 500 nm. Also, the fluorescence lifetime on the order of nanoseconds was obtained with a TCSPC system with pulsed excitation light at 507 nm

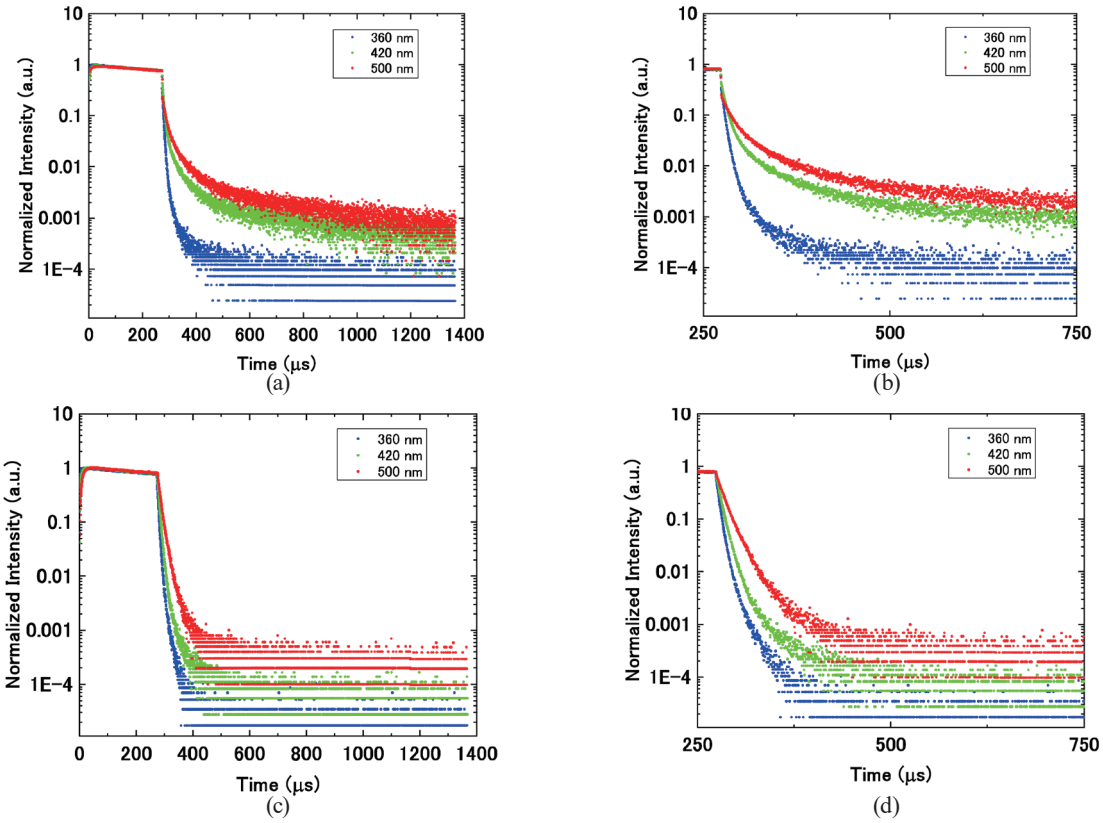


Fig. 5. (Color online) Comparison of optical attenuation curves of PG in microsecond scale obtained with an optical lifetime fluorometer with (a) aluminum impurity and (b) its expanded image, and (c) tin impurity and (b) its expanded image.

Table 1
Attenuation factors for Al: PG under ultraviolet excitation with 286 nm wavelength.

| Emission (nm) | $\tau_1$ (μs) | $\tau_2$ (μs) | $\tau_3$ (μs) | Average (μs) |
|---|---|---|---|---|
| 360 nm | 3.7 | 9.0 | 47.8 | 4.6 |
| (Contribution ratio) | (70.0%) | (25.2%) | (4.8%) | |
| 420 nm | 5.8 | 29.3 | 174.2 | 10.1 |
| (Contribution ratio) | (50.8%) | (31.7%) | (17.5%) | |
| 500 nm | 10.2 | 41.3 | 279.5.8 | 24.6 |
| (Contribution ratio) | (30.2%) | (41.5%) | (28.3%) | |

Table 2
Attenuation factors for Sn: PG under ultraviolet excitation with 286 nm wavelength.

| Emission (nm) | $\tau_1$ (μs) | $\tau_2$ (μs) | $\tau_3$ (μs) | Average (μs) |
|---|---|---|---|---|
| 360 nm | 3.6 | 7.1 | 20.8 | 4.4 |
| (Contribution ratio) | (65.2%) | (30.8%) | (4.0%) | |
| 420 nm | 4.9 | 9.5 | 44.6 | 6.3 |
| (Contribution ratio) | (54.7%) | (42.3%) | (2.9%) | |
| 500 nm | 9.1 | 20.0 | 114.4 | 11.2 |
| (Contribution ratio) | (66.2%) | (32.2%) | (1.7%) | |

wavelength. These differences between impurities are also visible in the TCSPC system with an emission wavelength of 560 nm. Figure 6 shows the difference in decay attenuation curve obtained for the emission wavelengths of 360 and 560 nm using the MCS and TCSPC systems, respectively.

### 3.3 Time-resolved fluorescence analysis

The time-resolved fluorometer enables us to obtain time-resolved emission spectra (TRES),[20] as shown in Figs. 7 and 8. Wavelength-dependent time-resolved decays are obtained as shown in Figs. 5 and 6. Through the time slice analysis of those multiple decay curves, TRES can be illustrated for each decay time span. Figure 7 shows the original and normalized TRES for Al: PG through the analysis of fluorescence attenuation curves in a wavelength range from 330 to 550 nm with an acquisition time of 120 s. The vertical axis of the attenuation curve corresponds to the spectral intensity for TRES and the horizontal axis represents the emission wavelength. The shape changes of the spectrum sliced every 6.3 μs were acquired from about 0.7 μs after the light source was cut off to 47 μs. Through TRES, the peak shift was observed on the long-wavelength side with the passage of time after the light source was cut off. It is considered that Al: PG has a fluorescent component with a relatively long life on the long-wavelength side.

The same TRES analysis was performed for Sn: PG and is illustrated in Fig. 8. The analysis targeted attenuation curves in the wavelength range from 330 to 550 nm. The acquisition time was set as 120 s. The shape changes of the spectrum sliced every 6.3 μs were acquired from about 0.7 μs after the light source was cut off to 47 μs. Through TRES, a similar peak shift was observed for Sn: PG as well. The comparison of the results of TRES analysis clearly showed that

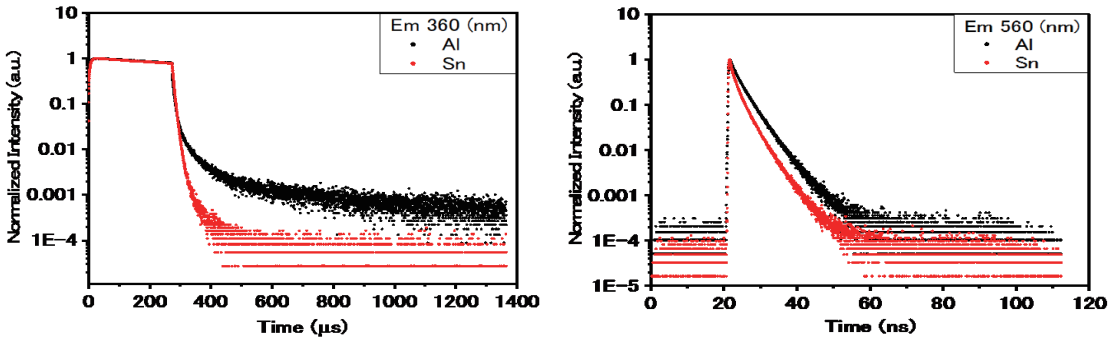


(a) (b)

Fig. 6. (Color online) Comparison of optical attenuation curves of PG with tin and aluminum impurities in (a) microsecond scale with emission wavelength of 360 nm (MCS) and (b) nanosecond scale with emission wavelength of 560 nm (TCSPC).

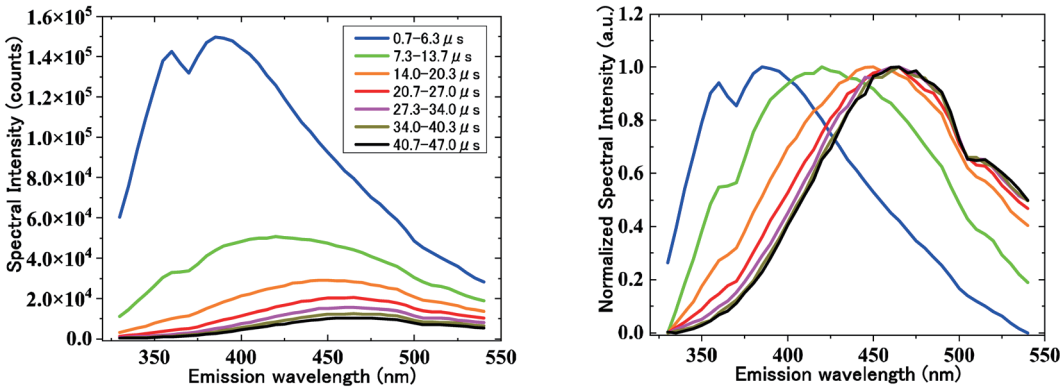


(a) (b)

Fig. 7. (Color online) (a) TRES and (b) normalized TRES of Al: PG in the wavelength range from 330 to 550 nm for attenuation time constants from 0.7 to 47.0 μs.

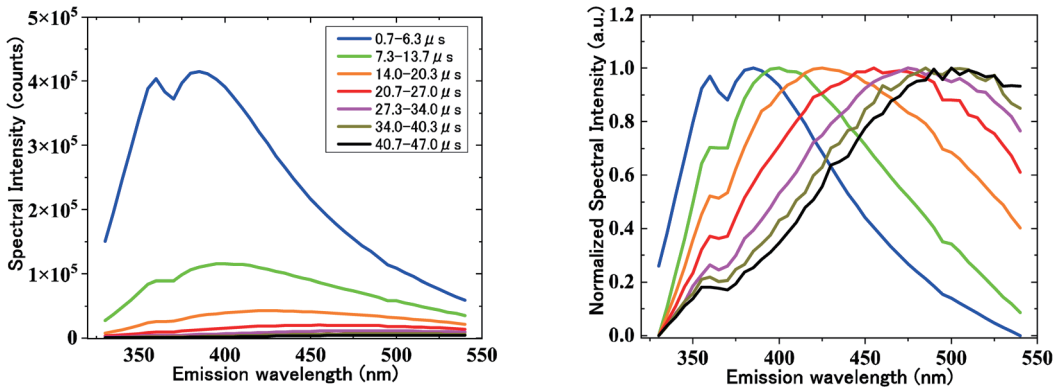


(a) (b)

Fig. 8. (Color online) (a) TRES and (b) normalized TRES of Sn: PG in the wavelength range from 330 to 550 nm for attenuation time constants from 0.7 to 47.0 μs.

Sn: PG has a longer lifetime for a longer wavelength than Al: PG; therefore, the origins of the two types of broadband fluorescence may be different from each other.

## 4. Discussion

The decay constant and TRES analysis suggest to us the difference in the origin of the broadband luminescence emitted from Al: PG and Sn: PG. The comparison of the decay curves for 360 nm showed that the long-lifetime component ($\tau_3$) contributes to illustrating the differences in both decay curves. It maintains a similar relationship with different emission wavelengths of 420 and 500 nm, although it is not illustrated in Fig. 6. TRES analysis is an effective tool for visualizing the origin of these differences in the wavelength-dispersive mode. Although similar spectra were obtained under the initial condition, Sn: PG and Al: PG showed different intensities of peak shift for the time span from 0.7 to 47 μs. Previous research suggested that Sn can form $Sn^{2+}$, which exhibits broadband white light emission in other types of glass crystal.[21–24] It may form similar or other color centers in the PG as well, as we see broadband luminescence from Sn: PG samples. Aluminum-related defects[25,26] may have their origin from the color center for broadband luminescence that corresponds to Al: PG samples. Since aluminum is included in the host crystal, there might be a particular concentration threshold to produce such color centers. Results indicated that the origin of the broadband luminescence is dependent on the impurities. However, it is subjected to an indirect analysis and may be ambiguous. Further chemical analysis, including elemental composition analysis such as secondary electron microscopy with energy-dispersive spectroscopy (SEM-EDS) or electron spin resonance (ESR), should be conducted to determine the origin and color centers created in PG. Moreover, transmittance should be measured, and the coincidence of the absorption and excitation wavelengths should be investigated further to identify the origin of the other luminescent centers that appeared in the data.

## 5. Conclusions

The optical properties of PG with two different impurities, namely, aluminum and tin, were investigated by fluorescence analysis. Broad white luminescence was observed from PGs with tin and aluminum impurities under deep ultraviolet exposure. Through emission and excitation spectroscopy and decay curve measurement, it is assumed that the origin of the broadband luminescence differs depending on the impurities introduced. In addition, TRES analysis was performed and spectroscopy at each decay time span was illustrated and compared. Results showed that the origin of the broadband luminescence is dependent on the impurities. Further chemical analysis should be carried out to determine the origin and color centers created in PG. Since aluminum is included in the host crystal, there might be a particular concentration threshold to produce such color centers. The RPL dosimeter utilizing silver-activated PG faces a thin film made of both aluminum and tin, which is used in energy-compensation filters. Therefore, the results obtained in this study might give important information about two potential impurities of PG for a better understanding of background noise and the functions of widely used radio-photoluminescence dosimeters.

## Acknowledgments

Part of this research was conducted in collaboration with the Chubu Electric Power Nuclear Safety Technology Center. The authors deeply thank Dr. T. Kurobori of Kanazawa University and Dr. K. Shinozaki of AIST for their support in the evaluation of fluorescence spectra. Considerable support was also provided by Taihei Chemical Industrial Co., Ltd., who provided the experimental sample powders used for RPL glass fabrication.

## References

1 J. H. Schulman, R. J. Ginther, C. C. Klick, R. S. Alger, and R. A. Levy: J. Appl. Phys. **22** (1951) 1479. https://doi.org/10.1063/1.1699896
2 R. Yokota and H. Imagawa: J. Phys. Soc. Jpn. **23** (1966) 1038. https://doi.org/10.1143/JPSJ.23.1038
3 T. Yamamoto, Y. Yanagida-Miyamoto, T. Iida, and H. Nanto: Rad. Meas. **136** (2020) 106363. https://doi.org/10.1016/j.radmeas.2020.106363
4 Ž. Knežević, L. Stolarczyk, I. Bessieres, J. M. Bordy, S. Miljanić, and P. Olko: Rad. Meas. **57** (2013) 9. https://doi.org/10.1016/j.radmeas.2013.03.004
5 Y. Miyamoto, T. Yamamoto, K. Kinoshita, S. Koyama, Y. Takei, H. Nanto, Y. Shimotsuma, M. Sakakura, K. Miura, and K. Hirao: Rad. Meas. **45** (2010) 546. https://doi.org/10.1016/j.radmeas.2010.01.012
6 J. A. Perry: Radiophotoluminescence in Health Physics (Adam Hilger, Bristol, 1987) pp. 28–66.
7 T. Kurobori, W. Zheng, Y. Miyamoto, H. Nanto, and T. Yamamoto: Opt. Mater. **32** (2010) 1231. https://doi.org/10.1016/j.optmat.2010.04.004
8 S. W. S. McKeever, S. Sholom, and N. Shrestha: Radiat. Meas. **123** (2019) 13. https://doi.org/10.1016/j.radmeas.2019.02.009
9 E. Piesch, B. Burgkhardt, M. Fischer, H. G. Röber, and S. Ugi: Radiat. Prot. Dos. **17** (1986) 293. https://doi.org/10.1093/oxfordjournals.rpd.a079826
10 T. Yamamoto, D. Maki, F. Sato, Y. Miyamoto, H. Nanto, and T. Iida: Radiat. Meas. **46** (2011) 1554. https://doi.org/10.1016/j.radmeas.2011.04.038
11 S. Koyama, Y. Miyamoto, A. Fujiwara, H. Kobayashi, K. Ajisawa, H. Komori, Y. Takei, H. Nanto, T. Kurobori, H. Kakimoto, M. Sakakura, Y. Shimotsuma, K. Miura, K. Hirao, and T. Yamamoto: Sens. Mater. **22** (2010) 377. https://doi.org/10.18494/SAM.2010.690
12 R. K. Parajuli, W. Kada, S. Kawabata, Y. Matsubara, K. Miura, A. Yokoyama, M. Haruyama, M. Sakai, and O. Hanaizumi: Key Eng. Mat. **698** (2016) 163. https://doi.org/10.4028/www.scientific.net/kem.698.163
13 R. Hashikawa, Y. Fujii, A. Kinomura, T. Saito, A. Okada, T. Wakasugi, and K. Kadono: J. Am. Ceram. Soc. **102** (2019) 1642. https://doi.org/10.1111/jace.16027
14 Y. Takada, K. Yamamoto, A. Kinomura, T. Saito, N. Ichinose, A. Okada, T. Wakasugi, and K. Kadono: A.I.P. Adv. **11** (2021) 035208. https://doi.org/10.1063/5.0044309
15 S. Kawabata, W. Kada, Y. Matsubara, T. Satoh, M. Sakai, R. K. Parajuli, N. Yamada, M. Koka, K. Miura, O. Hanaizumi, and T. Kamiya: Nucl. Instrum. Methods Phys. Res., Sect. B **406** (2017) 139. https://doi.org/10.1016/j.nimb.2017.04.017
16 S. Kawabata, W. Kada, R. K. Parajuli, Y. Matsubara, M. Sakai, K. Miura, T. Satoh, M. Koka, N. Yamada, T. Kamiya, and O. Hanaizumi: Jpn. J. Phys. **55** (2016) 06GD03. https://doi.org/10.7567/JJAP.55.06GD03
17 Taihei Chemical Industrial Co., Ltd: Private Communication (November, 2021).
18 Horiba Jobin Yvon IBH Ltd: A practical guide to time-resolved luminescence lifetime determination using dedicated time-correlated single-photon counting systems, https://www.horiba.com/fileadmin/uploads/Scientific/Downloads/UserArea/Fluorescence/Manuals/IBH-TCSPC-Guide.pdf (accessed October 2021).
19 Horiba Scientific Ltd: Time-resolved fluorescence lifetime measurements, https://static.horiba.com/fileadmin/Horiba/Products/Scientific/Molecular_and_Microanalysis/DeltaFlex/TechNote-1b-Time-resolved_fluorescence_lifetime_measurements.pdf (accessed November 2021).
20 Horiba Scientific Ltd: Time-resolved emission spectra/decay associated spectra, https://www.horiba.com/fileadmin/uploads/Scientific/Documents/Fluorescence/Tech_Note4_-_TRES-DAS.pdf (accessed October 2021).
21 H. Masai, T. Ina, S. Okumura, and K. Mibu: Sci. Rep. **8** (2018) 415. https://doi.org/10.1038/s41598-017-18847-0
22 H. Masai, Y. Ueda, T. Yanagida, G. Okada, and Y. Tokuda: Sens. Mater. **28** (2016) 871. https://doi.org/10.18494/SAM.2016.1354

23 A. Torimoto, H. Masai, G. Okada, and T. Yanagida: Sens. Mater. **29** (2017) 1383. https://doi.org/10.18494/SAM.2017.1617
24 M. Leskelä, T. Koskentalo, and G. Blasse: J. Solid State Chem. **59** (1985) 272. https://doi.org/10.1016/0022-4596(85)90294-4
25 V. Fuertes, J. F. Fernández, and E. Enríquez: Optica **6** (2019) 668. https://doi.org/10.1364/OPTICA.6.000668
26 A. I. Surdo, V. S. Kortov, V. A. Pustovarov, and V. Y. Yakovlev: Phys. Status Solidi C **2** (2005) 527. https://doi.org/10.1002/pssc.200460225